

# ULRR

## Asymptotic analysis for fiber drawing processes

|               |                                                                                                                               |
|---------------|-------------------------------------------------------------------------------------------------------------------------------|
| Item Type     | Article                                                                                                                       |
| Authors       | Hanevy, Niall;O'Kiely, Doireann                                                                                               |
| Citation      | SIAM Journal on Applied Mathematics. 83 (2), pp. 725-747                                                                      |
| Publisher     | Society for Industrial and Applied Mathematics                                                                                |
| Download date | 2026-05-08 14:24:47                                                                                                           |
| Item License  | <a href="https://creativecommons.org/licenses/by-nc-sa/4.0/">https://creativecommons.org/licenses/by-nc-sa/4.0/</a>           |
| Link to Item  | <a href="https://doi.org/10.34961/researchrepository-ul.23627706">https://doi.org/10.34961/researchrepository-ul.23627706</a> |

1        **ASYMPTOTIC ANALYSIS FOR FIBRE DRAWING PROCESSES\***

2                                NIALL HANEVY<sup>†</sup> AND DOIREANN O’KIELY<sup>‡</sup>

3        **Abstract.** In fibre drawing, axial tension is applied to long, thin viscous threads to increase  
4 their length and consequently reduce their cross-sectional area. This process is used to manufacture  
5 rods and threads of glass and polymer such as optical fibres and filaments for textiles. Drawing is  
6 described mathematically using the Trouton model for extensional flow in a long, narrow cylinder.  
7 This leading-order description gives simple expressions for fibre radius and one-dimensional axial  
8 velocity in the long, slender limit. In this paper we determine the next-order corrections, showing  
9 that they can be an order of magnitude larger than previously assumed.

10        **Key words.** example, L<sup>A</sup>T<sub>E</sub>X

11        **AMS subject classifications.** 68Q25, 68R10, 68U05

12        **1. Introduction.** Drawing is an umbrella term for a family of manufacturing  
13 processes in which threads, sheets and tubes of viscous or viscoelastic material are  
14 elongated. These processes are used in the manufacture of optical fibres [10, 29],  
15 filaments for textiles [18, 5], smartphone screens [20, 21, 22] and medical vials [11, 12,  
16 13]. The most common drawing process is fibre drawing. Here, a thread of material  
17 continually enters a stretching zone with a given radius and velocity. It is accelerated  
18 along the stretching zone, usually by rollers at the end of the stretching zone, which  
19 draw the thread away at a fixed velocity. This acceleration leads to a reduction in  
20 the thread radius, enabling the production of fibre-optic cables and polymer threads  
21 with diameters typically in the range 10–100µm [29, 5]. Many variations of the process  
22 exist: in magnet spinning, tension is applied to threads of a fluid containing magnetic  
23 nanoparticles by a rotating magnet [30], while tubes and microstructured optical fibres  
24 are manufactured by drawing fibres with internal holes, with pressure often used to  
25 maintain and control the hole size [8, 11].

26        A simple conservation-of-mass argument can be used to quantify the relationship  
27 between the velocity of a drawn fibre and its radius. For any fibre-drawing process  
28 operating in steady state, the flux of material in and out of the system must match,  
29 so if the cross-sectionally averaged axial velocity increases by a factor  $D$ , the cross-  
30 sectional area must decrease by a factor  $1/D$ . For a circular fibre with no internal  
31 holes, the radius must therefore decrease by a factor  $1/\sqrt{D}$ . The force required to  
32 attain this acceleration and the velocity profile along the stretching zone vary between  
33 systems and can be predicted using mathematical modelling. The fluid flow in fibre  
34 drawing is typically treated as a purely viscous flow, and is well-approximated by  
35 the one-dimensional *Trouton model* [31], with an axial velocity that is approximately  
36 uniform across the fibre radius. This model can be derived by exploiting the small  
37 aspect ratio  $\epsilon$  of radius to length of the fibre, either by assuming the fibre radius is  
38 slowly-varying [18] or via asymptotic expansion in the small aspect ratio [27]. Varia-  
39 tions on this approach have been used to investigate the stability of the steady state  
40 (i.e. draw resonance) [25, 15], to quantify the role of different effects such as gravity,  
41 inertia, surface tension and magnetism [18, 30] and to investigate the evolution of mi-

---

\*Submitted to the editors DATE.

<sup>†</sup>Department of Mathematics, College of Engineering and Physical Science, Aston University,  
UK (220360973@aston.ac.uk)

<sup>‡</sup>Department of Mathematics and Statistics, University of Limerick, Ireland (doireann.okiely@ul.ie, <http://www.doireannokiely.com>).

42 crostructure and cross-sectional profile [8, 11, 12, 20, 21]. Coupling between heat and  
 43 fluid flow is also a major point of interest in glass drawing processes, where elongation  
 44 is typically localized in the neighbourhood where temperature is highest and viscosity  
 45 is lowest [29, 28]. Stability is also a topic of major interest [24, 25, 15, 26].

46 Most of the modelling work carried out to date has involved either calculating  
 47 the leading-order behaviour in the limit as the aspect ratio  $\epsilon \rightarrow 0$  [18, 6], or numerical  
 48 solution of the two- or three-dimensional governing equations, e.g. [7]. Schultz &  
 49 Davis [27] extended the asymptotic expansion in powers of  $\epsilon^2$  and presented a calcula-  
 50 tion for correction terms at this order, while Page *et al.* [23] investigated adjustments  
 51 to the flow profile due to radially-dependent viscosity. However, recent analysis of  
 52 glass sheet redraw demonstrated that boundary layers at the sheet ends play a sig-  
 53 nificant role in determining corrections to the leading order, and can even give rise  
 54 to corrections which are actually  $O(\epsilon)$  [21]. In this paper we use a combination of  
 55 finite element and asymptotic analysis to analyse the correction terms in the case  
 56 of drawing of a circular fibre. We show that the first non-zero correction terms are  
 57  $O(\epsilon)$  for applied inlet and outlet velocities, an order of magnitude larger than those  
 58 calculated previously, and are  $O(\epsilon^2)$  for applied inlet and outlet stresses.

59 The paper is organized as follows. In Section 2 we outline the governing equations  
 60 for an axisymmetric viscous cylinder with fluid flow driven by either applied velocities  
 61 or applied stresses at inlet and outlet positions. We non-dimensionalize and introduce  
 62 an aspect ratio  $\epsilon$ . In Section 3 we present numerical solutions and highlight the rapid  
 63 adjustment of the flow profile between its one-dimensional bulk behaviour and the  
 64 applied conditions near the inlet and outlet in the case of applied velocities. In  
 65 Section 4 we present an asymptotic analysis of the long, slender limit  $\epsilon \rightarrow 0$ . We  
 66 reproduce the classic Trouton model at leading order. We introduce linear differential  
 67 equations for  $O(\epsilon)$  corrections whose solution may be non-zero if non-homogenous  
 68 boundary conditions are applied. Assessment of the leading-order solution reveals  
 69 boundary layers at the fibre ends, which are analysed in Section 5. This boundary-  
 70 layer analysis both resolves the rapid adjustment of the leading-order solution near  
 71 the inlet and outlet and yields correct boundary conditions for the  $O(\epsilon)$  corrections.  
 72 Crucially, these boundary conditions are non-homogenous, and  $O(\epsilon)$  corrections to  
 73 the leading-order Trouton model are predicted. These corrections are presented in  
 74 Section 6 and are in excellent agreement with numerical solutions. We conclude  
 75 by discussing alternative boundary conditions and temperature effects in Sections 7  
 76 and 8, followed by a discussion in Section 9.

## 77 2. Governing equations.

78 **2.1. Two-dimensional axisymmetric model.** We consider steady-state, axi-  
 79 symmetric drawing of a thread of Newtonian fluid, and assume that inertia and  
 80 gravity are negligible. We neglect temperature effects and assume that the fibre has  
 81 a uniform viscosity  $\mu^*$ , although the analysis presented here can be extended to an  
 82 axially-varying viscosity as outlined in Appendix A. We use cylindrical polar coordi-  
 83 nates centered in the middle of the fibre at the beginning of the draw zone, with  $z^*$   
 84 pointing along the fibre axis in the direction of fibre drawing and  $r^*$  pointing in the  
 85 radial direction as shown in Figure 1. We denote the radial and axial velocities by  $u^*$   
 86 and  $w^*$  respectively, and the pressure by  $p^*$ . Conservation of mass and momentum in

87 the fibre are described by

88 (2.1) 
$$\frac{1}{r^*} \frac{\partial}{\partial r^*} (r^* u^*) + \frac{\partial w^*}{\partial z^*} = 0,$$

89 (2.2) 
$$-\frac{\partial p^*}{\partial r^*} + \mu^* \frac{\partial}{\partial r^*} \left[ \frac{1}{r^*} \frac{\partial}{\partial r^*} (r^* u^*) \right] + \mu^* \frac{\partial^2 u^*}{\partial z^{*2}} = 0,$$

90 (2.3) 
$$-\frac{\partial p^*}{\partial z^*} + \mu^* \frac{1}{r^*} \frac{\partial}{\partial r^*} \left( r^* \frac{\partial w^*}{\partial r^*} \right) + \mu^* \frac{\partial^2 w^*}{\partial z^{*2}} = 0,$$

92 where the radial momentum equation (2.2) includes a contribution from the axisym-  
 93 metric hoop stress  $-p^* + 2\mu^* u^*/r^*$ . The fibre radius is not known *a priori* and must be  
 94 determined as part of the problem solution; we denote it by  $r^* = R^*(z^*)$ . We impose  
 95 no-flux and no-stress conditions (neglecting surface tension) at this free boundary via

96 (2.4) 
$$u^* = \frac{dR^*}{dz^*} w^*,$$

97 (2.5) 
$$\left( -p^* + 2\mu^* \frac{\partial u^*}{\partial r^*} \right) = \frac{dR^*}{dz^*} \left[ \mu^* \left( \frac{\partial w^*}{\partial r^*} + \frac{\partial u^*}{\partial z^*} \right) \right],$$

98 (2.6) 
$$\mu^* \left( \frac{\partial w^*}{\partial r^*} + \frac{\partial u^*}{\partial z^*} \right) = \frac{dR^*}{dz^*} \left( -p^* + 2\mu^* \frac{\partial w^*}{\partial z^*} \right),$$

100 at  $r^* = R^*(z^*)$ .

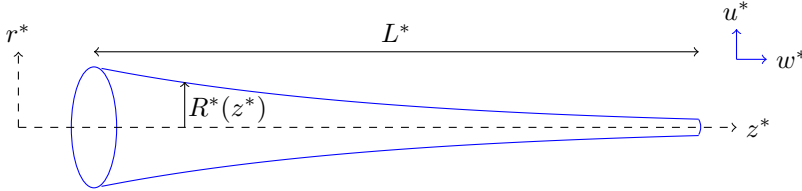


Fig. 1: Schematic of fibre drawing

101 **2.2. Inlet and outlet conditions.** The fibre enters the drawing zone at a  
 102 known radius

103 (2.7) 
$$R^*(0) = R_{in}^*.$$

104 The acceleration required for thinning of the viscous thread is driven by a mismatch  
 105 between velocities imposed at the inlet and outlet to the stretching zone: increasing  
 106 the axial velocity by a factor  $D$  leads to a reduction in radius by a factor  $1/\sqrt{D}$ . The  
 107 mechanism by which material enters the stretching zone varies between industries: for  
 108 fibre-optic cables, a solid cylinder known as a preform is fed into a furnace where it is  
 109 heated and stretched, while for polymer drawing, liquid polymer is usually extruded  
 110 through a die into the stretching zone. At the outlet, the material exits the stretching  
 111 zone at an outlet velocity that is larger than the inlet velocity, which may be controlled  
 112 directly or via an applied tension. We consider three different scenarios:

113 1. Uniform velocity: the fibre enters and exits the stretching zone via rigid body  
 114 translation, and a pressure condition is applied to close the problem, so

115 (2.8a) 
$$w^* = w_{in}^*, \quad u^* = 0 \quad \text{at} \quad z^* = 0,$$

116

$$(2.8b) \quad p^* = 0 \quad \text{at} \quad z^* = 0,$$

118

$$(2.8c) \quad w^* = w_{\text{out}}^*, \quad u^* = 0 \quad \text{at} \quad z^* = L^*,$$

120

where  $w_{\text{in}}^*$  and  $w_{\text{out}}^*$  are the inlet and outlet velocities and  $L^*$  is the length of the stretching zone.

121

2. Applied tension: a uniform axial stress and zero shear stress are applied at the inlet and outlet, and a uniform inlet axial velocity is applied to close the problem, so

122

$$(2.9a) \quad \left. \begin{aligned} \sigma_{zz}^* &= -p^* + 2\mu^* \frac{\partial w^*}{\partial z^*} = \sigma_{\text{in}}^*, \\ \sigma_{rz}^* &= \mu^* \left( \frac{\partial u^*}{\partial z^*} + \frac{\partial w^*}{\partial r^*} \right) = 0 \\ w^* &= w_{\text{in}}^* \end{aligned} \right\} \quad \text{at} \quad z^* = 0,$$

126

$$(2.9b) \quad \left. \begin{aligned} \sigma_{zz}^* &= -p^* + 2\mu^* \frac{\partial w^*}{\partial z^*} = \sigma_{\text{out}}^*, \\ \sigma_{rz}^* &= \mu^* \left( \frac{\partial u^*}{\partial z^*} + \frac{\partial w^*}{\partial r^*} \right) = 0 \end{aligned} \right\} \quad \text{at} \quad z^* = L^*,$$

127

128

3. Pipe flow: for die extrusion the fibre enters through a tube and may have a radially-varying axial velocity, e.g. Poiseuille; in this case we might impose

129

$$(2.10) \quad w^* = 2w_{\text{in}}^* \left( 1 - \frac{r^2}{(R_{\text{in}}^*)^2} \right), \quad u^* = 0 \quad \text{at} \quad z^* = 0.$$

130

131

together with an inlet pressure and either uniform velocity or applied stress outlet conditions.

132

Combinations of these conditions could also be applied, but we focus here on cases 1 and 2, and radially-varying inlet profiles are discussed briefly in §7.

133

**2.3. Non-dimensionalization.** We non-dimensionalize by defining  $\epsilon = R_{\text{in}}^*/L^*$  and introducing

134

(2.11a)

$$(2.11a) \quad (z, r) = \left( \frac{z^*}{L^*}, \frac{r^*}{\epsilon L^*} \right), \quad (w, u) = \left( \frac{w^*}{w_{\text{in}}^*}, \frac{u^*}{\epsilon w_{\text{in}}^*} \right), \quad p = \frac{p^*}{\mu^* w_{\text{in}}^* / L^*}, \quad R = \frac{R^*}{R_{\text{in}}^*}.$$

137

138

$$(2.11b) \quad p = \frac{p^*}{\mu^* w_{\text{in}}^* / L^*}, \quad \sigma_{ii} = \frac{\sigma_{ii}^*}{\mu^* w_{\text{in}}^* / L^*}, \quad \sigma_{rz} = \frac{\sigma_{rz}^*}{\epsilon^{-1} \mu^* w_{\text{in}}^* / L^*}.$$

139

Substituting these dimensionless variables into the governing equations (2.1)–(2.8a) yields mass and momentum equations

140

$$(2.12) \quad \frac{1}{r} \frac{\partial}{\partial r} (ru) + \frac{\partial w}{\partial z} = 0,$$

142

$$(2.13) \quad -\frac{\partial p}{\partial r} + \frac{\partial}{\partial r} \left[ \frac{1}{r} \frac{\partial}{\partial r} (ru) \right] + \epsilon^2 \frac{\partial^2 u}{\partial z^2} = 0,$$

143

$$(2.14) \quad -\frac{\partial p}{\partial z} + \epsilon^{-2} \frac{1}{r} \frac{\partial}{\partial r} \left( r \frac{\partial w}{\partial r} \right) + \frac{\partial^2 w}{\partial z^2} = 0,$$

144

145

146 together with free-boundary conditions

$$147 \quad (2.15) \quad u = \frac{dR}{dz} w,$$

$$148 \quad (2.16) \quad -p + 2 \frac{\partial u}{\partial r} = \frac{dR}{dz} \left( \frac{\partial w}{\partial r} + \epsilon^2 \frac{\partial u}{\partial z} \right),$$

$$149 \quad (2.17) \quad \epsilon^{-2} \frac{\partial w}{\partial r} + \frac{\partial u}{\partial z} = \frac{dR}{dz} \left( -p + 2 \frac{\partial w}{\partial z} \right),$$

151 at  $r = R(z)$ . We also require all quantities to be regular at  $r = 0$ ; so the radial  
152 velocity and (axisymmetric) shear stress are both zero there.

153 For applied inlet and outlet velocities (case 1), we obtain

$$154 \quad (2.18) \quad w = R = 1, \quad u = p = 0, \quad \text{at } z = 0,$$

$$155 \quad (2.19) \quad w = D, \quad u = 0 \quad \text{at } z = 1,$$

157 where  $D = w_{\text{out}}^*/w_{\text{in}}^*$  is referred to as the draw ratio. For applied inlet and outlet  
158 stresses (case 2), we obtain

$$159 \quad (2.20a) \quad w = R = 1 \quad \text{at } z = 0,$$

160

$$161 \quad (2.20b) \quad \sigma_{zz} = -p + 2 \frac{\partial w}{\partial z} = \sigma_{\text{in}}, \quad \sigma_{rz} = \epsilon^2 \frac{\partial u}{\partial z} + \frac{\partial w}{\partial r} = 0 \quad \text{at } z = 0,$$

162

$$163 \quad (2.20c) \quad \sigma_{zz} = -p + 2 \frac{\partial w}{\partial z} = \sigma_{\text{out}}, \quad \sigma_{rz} = \epsilon^2 \frac{\partial u}{\partial z} + \frac{\partial w}{\partial r} = 0 \quad \text{at } z = 1,$$

164 where  $\sigma_{\text{in}} = \sigma_{\text{in}}^* L^*/\mu^* w_{\text{in}}^*$  and  $\sigma_{\text{out}} = \sigma_{\text{out}}^* L^*/\mu^* w_{\text{in}}^*$  are dimensionless axial stresses,  
165 which must be chosen to give a desired increase in axial velocity.

166 **2.4. Averaged quantities.** In §4 we will also utilize cross-sectionally averaged  
167 versions of the mass and axial momentum equations. These are obtained by integrat-  
168 ing (2.12) and (2.14) across the fibre radius and applying the no-flux and no-stress  
169 boundary conditions (2.15) and (2.17). We do the second calculation by first rewrit-  
170 ing (2.14) in terms of  $-p + 2\partial w/\partial z$  and  $\partial u/\partial z + \partial w/\partial r$  using (2.12). We then find

$$171 \quad (2.21) \quad \frac{d}{dz} \int_0^{R(z)} r w \, dr = 0,$$

$$172 \quad (2.22) \quad \frac{d}{dz} \int_0^{R(z)} r \left[ -p + 2 \frac{\partial w}{\partial z} \right] \, dr = 0.$$

173

174 **3. Numerical solution.** We solve the full two-dimensional problem (2.12)—  
175 (2.17) numerically using the finite-element software FEniCS [17], mapping the prob-  
176 lem onto a fixed domain via a change of variables [16, 4, 21].

$$177 \quad (3.1) \quad \eta = \frac{r}{R(z)}, \quad \zeta = z.$$

178 The domain  $[\eta, \zeta] \in [0, 1] \times [0, 1]$  is triangulated using a  $100 \times 96$  mesh for  $\zeta \in [0.2, 0.98]$   
179 and 16 times higher resolution in  $\zeta$  for  $\zeta \in [0, 0.2]$  and  $\zeta \in [0.98, 1]$ . The increased  
180 resolution near the inlet and outlet was required to accurately resolve rapid changes

181 in the solution in these zones. The numerical scheme used quadratic test functions for  
 182 velocity components and fibre radius and a linear test function for pressure. Further  
 183 details of the solution procedure are given in Appendix B

184 Plots of the numerical solution are shown in Figure 2 for case 1, i.e. applied  
 185 velocities. A draw ratio  $D = 30$  and aspect ratio  $\epsilon = 0.1$  was used in this case,  
 186 but the solutions for other values of  $D$  and of  $\epsilon \ll 1$  are similar. Solutions for  
 187 cases 1 and 2 are shown together in Figure 3, with stresses  $\sigma_{\text{in}}^* = 3 \log(30)$  and  
 188  $\sigma_{\text{out}}^* = 3 \times 30 \log(30)$  which will be justified in §4.1. The solutions are very similar apart  
 189 from in small regions near the boundaries. In Figure 2, the velocity in the  $z$ -direction  
 190 is approximately uniform across the fibre radius, and increases from  $w(r, 0) = 1$   
 191 at the inlet to  $w(r, 1) = 30$  at the outlet, as required by the boundary conditions  
 192 (see a). The fibre radius decreases (highlighted in b) from  $R(0) = 1$  to  $R(1) =$   
 193  $1/\sqrt{30} \approx 0.18$  as expected. The transverse velocity is directed radially inward (see  
 194 c), which is consistent with a decreasing fibre radius, and its magnitude appears to  
 195 increase linearly with distance from the central axis (see inset). The radial velocity  
 196 and pressure both exhibit rapid changes near the inlet and outlet for applied velocities  
 197 (see c and d, or Figure 3 c and d), but not for applied tensions; we will analyse this  
 198 further via asymptotic analysis below. We also note that applying a velocity boundary  
 199 condition at the outlet leads to a pressure singularity at the corner  $z = 1, r = R(1)$ .  
 200 Such a singularity is common when there is a sudden change in boundary conditions,  
 201 see e.g. [9], and we note that it disappears when stress conditions are applied instead.

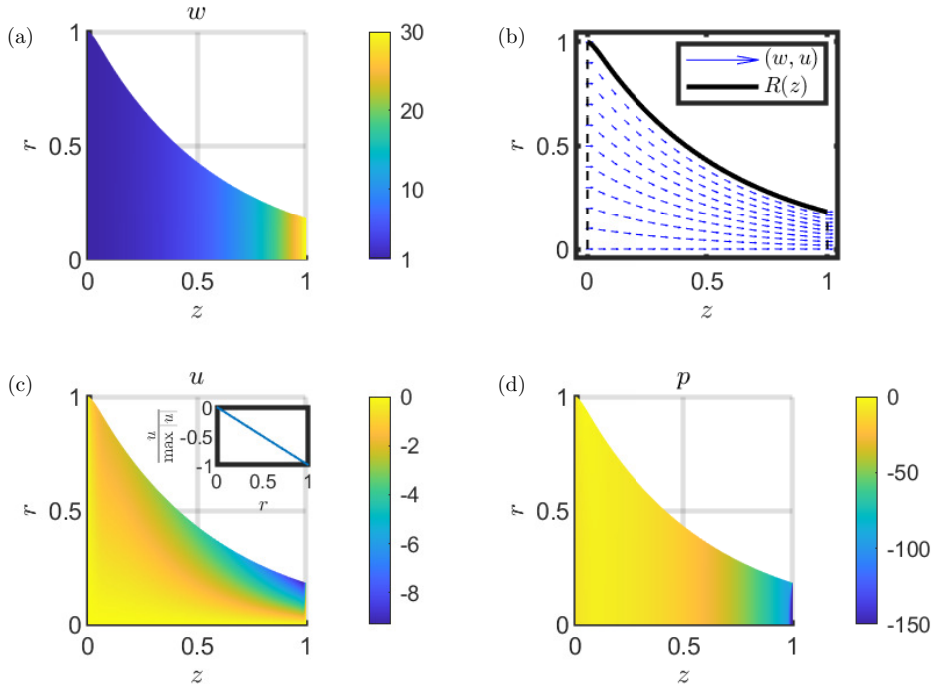


Fig. 2: Numerical solution to fibre-drawing equations (2.12)–(2.19), with velocity boundary conditions (case 1), for draw ratio  $D = 30$  and aspect ratio  $\epsilon = 0.1$ : (a) axial velocity, (b) flow profile, with fibre radius  $R(z)$  highlighted in black, (c) radial velocity, with  $u$  evaluated at  $z = 0.5$  in the inset, and (d) pressure.

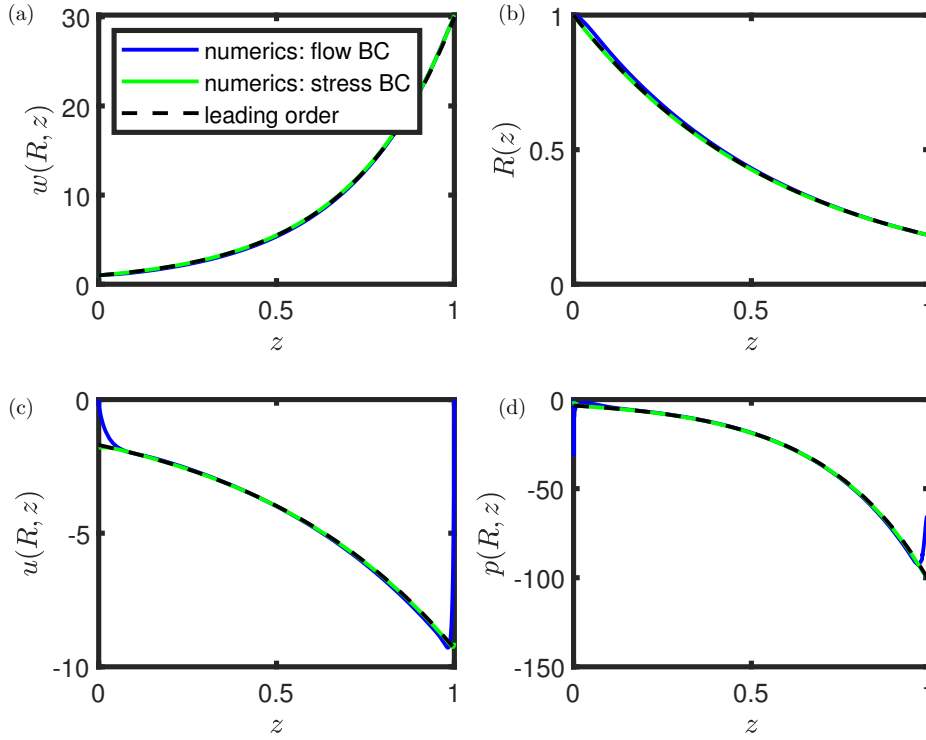


Fig. 3: Leading-order solutions for velocity, pressure and fibre radius, compared with numerical solutions evaluated on the fibre surface for  $\epsilon = 0.1$ ,  $D = 30$ .

202 **4. Asymptotic analysis.** We exploit the fact that the aspect ratio  $\epsilon$  is small  
 203 by expanding the pressure, velocities, and fibre radius in powers of  $\epsilon$  and taking the  
 204 limit  $\epsilon \rightarrow 0$ . The radial velocity, for example, is rewritten as

$$205 \quad u = u_0 + \epsilon u_1 + \epsilon^2 u_2 + \epsilon^3 u_3 + \dots$$

207 The derivation outlined below for the leading-order quantities is standard, and can  
 208 found throughout the literature, for example in [27, 6, 14, 8]. However, here an  
 209 analogous derivation for the  $O(\epsilon)$  terms is also carried out. The procedure is the same  
 210 at both orders so the two are carried out together.

211 **4.1. Bulk equations.** Evaluating the axial momentum equation (2.14) and cor-  
 212 responding boundary condition (2.17) at  $O(1)$  immediately yields the result that the  
 213 axial velocity does not vary with radius up to  $O(\epsilon^2)$ , i.e.

$$214 \quad (4.1) \quad w_0 = W_0(z), \quad w_1 = W_1(z).$$

215 It then follows from the continuity equation (2.12) that the radial velocity is linear in  
 216  $r$  at these orders, i.e.

$$217 \quad (4.2) \quad u_0 = -\frac{r}{2}W_0'(z), \quad u_1 = -\frac{r}{2}W_1'(z),$$

218 where we have used the requirement of zero radial velocity at the centre of the fibre  
 219 to determine the constants of integration. These profiles are consistent with the

numerical solutions presented in §3. Following a similar procedure with the radial momentum equation (2.13) and corresponding boundary condition (2.16) yields

$$(4.3) \quad p_0 = -W_0'(z), \quad p_1 = -W_1'(z),$$

so the pressure is approximately uniform across the sheet thickness and is related directly to the velocity gradient. We can now close the problem for the functions  $W_0$  and  $R_0$  by evaluating the averaged equations (2.21) and (2.22) at leading order to find

$$(4.4) \quad \frac{d}{dz} (R_0^2 W_0) = 0, \quad \frac{d}{dz} (3R_0^2 W_0') = 0.$$

Integrating the leading-order equations (4.4) and applying the inlet and outlet conditions (2.18) and (2.19) yields

$$(4.5) \quad W_0(z) = D^z, \quad R_0(z) = D^{-z/2}.$$

The same solution is obtained for the inlet and outlet conditions (2.20a)–(2.20c) if the stresses are chosen to be  $\sigma_{\text{in}} = 3 \ln(D)$  and  $\sigma_{\text{out}} = 3D \ln(D)$ .

The full leading-order solution is therefore

$$(4.6) \quad w_0 = D^z,$$

$$(4.7) \quad R_0 = D^{-z/2},$$

$$(4.8) \quad u_0 = -\frac{r}{2} \ln(D) D^z,$$

$$(4.9) \quad p_0 = -\ln(D) D^z.$$

We compare the leading-order solution (4.6)–(4.9) to the numerical solution from §3 in Figure 3 for an aspect ratio  $\epsilon = 0.1$  and draw ratio  $D = 30$ . The fibre radius and axial velocity are in excellent agreement with the numerical solutions throughout the domain. The radial velocity and pressure are also in good agreement, except for small regions near the inlet and outlet in the case of an applied inlet and outlet velocity field, where the numerical solution adjusts rapidly to satisfy the boundary conditions. We note here that the leading-order radial velocity  $u_0 = -(r/2)w_0'(z) = -(r/2) \ln(D) D^z$  and pressure  $p_0 = -w_0'(z) = -\ln(D) D^z$  follow directly from the axial velocity profile and cannot satisfy general inlet and outlet conditions, including the conditions (2.18)–(2.19) for an applied velocity field. This suggests that there are two-dimensional boundary layers near the inlet and outlet where the fluid velocity adjusts from the imposed boundary conditions to the one-dimensional bulk solution. We analyse these boundary layers in §5.1–5.3.

We can repeat the derivation procedure outlined above to find governing equations for the  $O(\epsilon)$  variables by evaluating the averaged equations (2.21), (2.22) to give

$$(4.10) \quad \frac{d}{dz} (R_0^2 W_1 + 2R_0 R_1 W_0) = 0, \quad \frac{d}{dz} [3(R_0^2 W_1' + 2R_0 R_1 W_0')] = 0,$$

where the prime (') denotes differentiation with respect to  $z$ . If we solved these equations subject to  $R_1 = W_1 = 0$  at the inlet and outlet, we would find that the  $O(\epsilon)$  corrections are identically zero. However, the occurrence of boundary layers near  $z = 0$  and  $z = 1$  suggests that there may be non-zero boundary conditions and hence non-zero corrections; we investigate this further in §5.

260 **4.2. Error quantification.** We analyse the performance of the leading-order  
 261 solution (4.6)–(4.9) by calculating the error compared with the numerical solution  
 262 from §3 see Figure 4. The deviation from leading-order is larger for case 1 than case  
 263 2, and neither is captured accurately by the Schultz & Davis [27] prediction

$$264 \quad (4.11) \quad R_{\text{SD}}(z) = D^{-z/2} + \epsilon^2 \frac{(\ln D)^2}{16} \left[ z \left( 1 - \frac{1}{D} \right) - \left( 1 - \frac{1}{D^z} \right) \right] D^{-z/2} + O(\epsilon^4),$$

$$265 \quad (4.12) \quad w_{\text{SD}}(r, z) = D^z + \epsilon^2 \frac{(\ln D)^2}{8} \left\{ \left[ -4r^2 + 1 - z \left( 1 - \frac{1}{D} \right) \right] D^z + 1 \right\} + O(\epsilon^4).$$

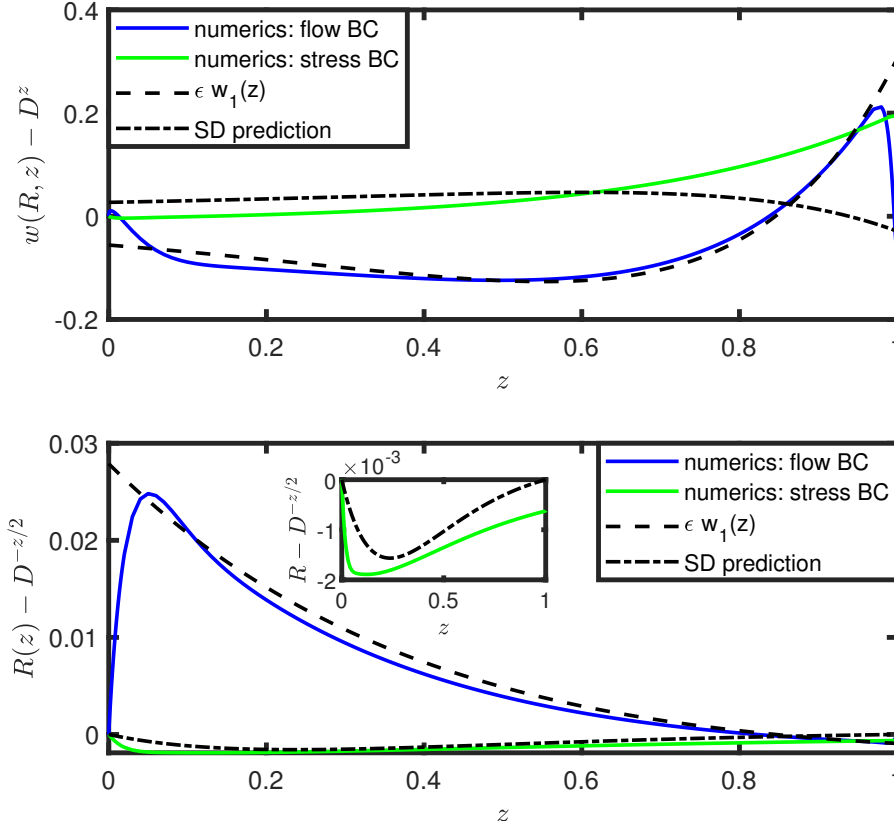


Fig. 4: Corrections to the leading-order predictions  $w \approx D^z$  and  $R \approx D^{-z/2}$  for  $\epsilon = 0.05$ : the numerical solution from §3 is compared to the asymptotic solutions  $\epsilon w_1$  and  $\epsilon R_1$  given by (6.5) and (6.6) respectively. The  $O(\epsilon^2)$  prediction from [27] is included for reference.

267 We investigate further by examining the size of the deviation as a function of  
 268 the small aspect ratio  $\epsilon$ ; for simplicity we evaluate on the free boundary at particular  
 269 values of  $z$  that are not near sign changes in error. We carry out the calculation for  
 270 three different mesh densities to ensure numerical convergence. The error increases  
 271 linearly with  $\epsilon$  in the case of applied velocity fields, and quadratically with  $\epsilon$  in  
 272 the case of applied stress fields. This suggests that the first corrections in the asymp-  
 273 totic expansion should be of  $O(\epsilon)$  for at least some boundary conditions, which is in

274 contrast to [27] where corrections are assumed to be  $O(\epsilon^2)$ . Since applied velocity  
 275 fields correspond to a worst-case scenario with  $O(\epsilon)$  deviations from leading order, we  
 276 concentrate on modelling and explaining that scenario in the sections below.

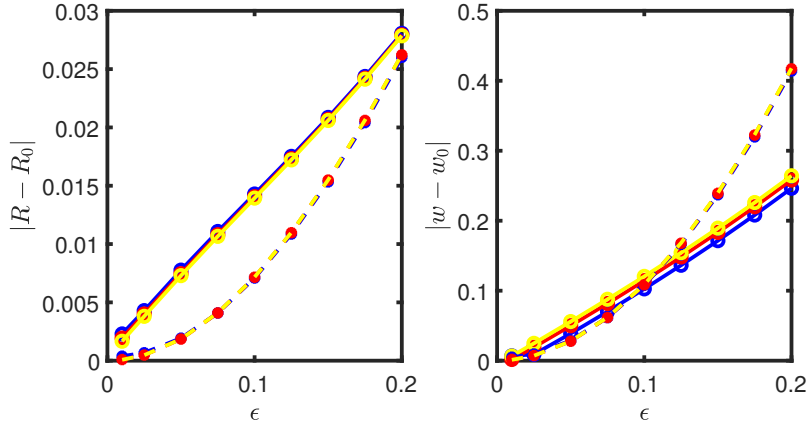


Fig. 5: Errors in the leading-order Trouton model (4.6)–(4.9) compared to the numerical solution to (2.12)–(2.17). The axial velocity is evaluated on the free boundary at  $z = 0.5$  while the fibre radius is evaluated at  $z = 0.2$ . The three colours correspond to three mesh densities: blue is the mesh described in §3, red has 1/2 as many mesh points and yellow has 1/4 as many mesh points. The solid curves are for case 1, i.e. inlet and outlet velocity conditions, while the dashed curves are for case 2, i.e. inlet and outlet stress conditions.

## 277 5. Boundary-layer analysis.

278 **5.1. Inlet boundary layer.** Since the one-dimensional leading-order solution  
 279 (4.8) cannot satisfy an inlet boundary condition  $u_0(0) = 0$ , we consider a boundary  
 280 layer of size  $\epsilon$  where two-dimensional effects will appear at leading order. We rescale  
 281 into this boundary layer by defining

$$282 \quad (5.1) \quad z = \epsilon \bar{z}, \quad r = \bar{r}.$$

283 We anticipate matching the boundary-layer solution as  $\bar{z} \rightarrow \infty$  to the bulk solu-  
 284 tion (4.6)–(4.9) as  $z \rightarrow 0$ , so we propose boundary-layer solutions of the form

$$285 \quad (5.2) \quad w(r, z) = 1 + \epsilon \ln(D) (\bar{z} + \bar{w}(\bar{r}, \bar{z})) + \dots,$$

$$286 \quad (5.3) \quad R(z) = 1 + \epsilon \ln(D) \left( -\frac{\bar{z}}{2} + \bar{R}(\bar{z}) \right) + \dots,$$

$$287 \quad (5.4) \quad u(r, z) = \ln(D) \left( -\frac{\bar{r}}{2} + \bar{u}(\bar{r}, \bar{z}) \right) + \dots,$$

$$288 \quad (5.5) \quad p(r, z) = \ln(D) (-1 + \bar{p}(\bar{r}, \bar{z})) + \dots.$$

290 We now substitute the change of variables and expansion into the full dimension-  
 291 less problem (2.12)–(2.17). This results in a canonical leading-order boundary-layer

292 problem

$$293 \quad (5.6) \quad \frac{1}{\bar{r}} \frac{\partial}{\partial \bar{r}} (\bar{r} \bar{u}) + \frac{\partial \bar{w}}{\partial \bar{z}} = 0,$$

$$294 \quad (5.7) \quad -\frac{\partial \bar{p}}{\partial \bar{r}} + \frac{\partial}{\partial \bar{r}} \left[ \frac{1}{\bar{r}} \frac{\partial}{\partial \bar{r}} (\bar{r} \bar{u}) \right] + \frac{\partial^2 \bar{u}}{\partial \bar{z}^2} = 0,$$

$$295 \quad (5.8) \quad -\frac{\partial \bar{p}}{\partial \bar{z}} + \frac{1}{\bar{r}} \frac{\partial}{\partial \bar{r}} \left( \bar{r} \frac{\partial \bar{w}}{\partial \bar{r}} \right) + \frac{\partial^2 \bar{w}}{\partial \bar{z}^2} = 0.$$

297 Since the free boundary is located at  $\bar{r} = r = R = 1 + O(\epsilon)$ , the conditions there can  
298 be linearized onto  $\bar{r} = 1$ , and so the no-stress conditions there yield

$$299 \quad (5.9) \quad -\bar{p} + 2 \frac{\partial \bar{u}}{\partial \bar{r}} = 0,$$

$$300 \quad (5.10) \quad \frac{\partial \bar{w}}{\partial \bar{r}} + \frac{\partial \bar{u}}{\partial \bar{z}} = 0.$$

302 The corresponding inlet and far-field conditions are given by

$$303 \quad (5.11) \quad \bar{w} = 0, \quad \bar{u} = \frac{\bar{r}}{2}, \quad \bar{p} = 1 \quad \text{at} \quad \bar{z} = 0,$$

$$304 \quad (5.12) \quad \bar{u}, \bar{p} \rightarrow 0 \quad \text{as} \quad \bar{z} \rightarrow \infty.$$

306 The correction to the fibre radius inside the boundary layer is then given by

$$307 \quad (5.13) \quad \frac{d\bar{R}}{d\bar{z}} = \bar{u}(1, \bar{z}), \quad \bar{R}(\bar{z} = 0) = 0.$$

308 This boundary-layer problem must be solved numerically, but is independent of the  
309 draw ratio  $D$ , so it only needs to be solved once and the solution can then be rescaled  
310 for any draw ratio and aspect ratio. We carry out the numerical solution in §5.3, but  
311 we first derive the governing equations in the boundary layer near the outlet.

312 **5.2. Outlet boundary layer.** In the boundary layer near the outlet we an-  
313 ticipate that the fibre radius will be approximately  $1/\sqrt{D}$ , so we rescale into the  
314 boundary layer and simultaneously scale the governing equations onto a domain of  
315 radius 1 by defining

$$316 \quad (5.14) \quad z = 1 - \epsilon D^{-1/2} \bar{z}, \quad r = D^{-1/2} \bar{r}.$$

317 We re-use the bar notation from §5.1 in anticipation that the inlet and outlet zones  
318 will correspond to scaled versions of the same system. Inspired by the canonical  
319 inlet problem derived in §5.1, we aim to eliminate the draw ratio from the governing  
320 equations. To this end, we carry out a boundary-layer rescaling for the velocity and  
321 pressure

$$322 \quad (5.15) \quad w(r, z) = D \left[ 1 - \epsilon D^{-1/2} \ln(D) (\bar{z} + \bar{w}(\bar{r}, \bar{z})) + \dots \right],$$

$$323 \quad (5.16) \quad R(z) = D^{-1/2} \left[ 1 - \epsilon D^{-1/2} \ln(D) \left( -\frac{\bar{z}}{2} + \bar{R}(\bar{z}) + c_{out} \right) + \dots \right],$$

$$324 \quad (5.17) \quad u(r, z) = D^{1/2} \ln(D) \left( -\frac{\bar{r}}{2} + \bar{u}(\bar{r}, \bar{z}) \right) + \dots,$$

$$325 \quad (5.18) \quad p(r, z) = D \ln(D) (-1 + \bar{p}(\bar{r}, \bar{z})) + \dots,$$

327 where repeated use of barred variables and the inclusion of the constant  $c_{out}$  in the  
 328 expansion for  $R$  will both be explained below. Substituting the expansion (5.15)—  
 329 (5.18) into the governing equations (2.12)—(2.17) yields the same governing equa-  
 330 tions (5.6)—(5.13) for the outlet boundary layer as for the inlet boundary layer. The  
 331 fibre radius is not imposed at the outlet so we do not immediately have a boundary  
 332 condition at  $\bar{z} = 0$ . Ultimately, the fibre radius in the boundary layer will be required  
 333 to match the fibre radius in the bulk as  $z \rightarrow 1$ , which we will calculate in §6. For now,  
 334 we close the problem under consideration here by introducing an offset  $c_{out}$  such that  
 335  $\bar{R}(0) = 0$  and the outlet problem matches the inlet one exactly. We anticipate that  
 336  $c_{out} = 0$  since the final radius should be exactly  $1/\sqrt{D}$  by conservation of mass, but  
 337 we confirm this in §6.

338 The inflow and outflow boundary layers are now described in terms of a single  
 339 canonical boundary-layer problem (5.6)—(5.13).

340 **5.3. Numerical solution.** The canonical boundary layer problem (5.6)—(5.13)  
 341 was solved numerically using FEniCS [17]. We note that the problem is defined  
 342 on a fixed but semi-infinite domain  $\bar{r} \in [0, 1]$ ,  $\bar{z} \in [0, \infty)$ , which was truncated for  
 343 the numerical solution at  $\bar{z} = 10$ . The numerical solutions are shown in Figure 6,  
 344 truncated at  $\bar{z} = 3$  for visibility. We observe that both velocity components vary in  
 345 both directions inside the boundary layer. The correction to the fibre radius exhibits a  
 346 slight bump, associated with the slight decrease in axial velocity as the radial velocity  
 347 adjusts to its bulk profile. We note that the pressure exhibits a singularity at  $\bar{z} = 0$ ,  
 348  $\bar{r} = 1$ : this corresponds to the singularities at  $z = 0$  and  $z = 1$  in the solution of the  
 349 full problem (Fig. 3).

350 **5.4. Far-field behaviour.** We will determine the corrections to the bulk solu-  
 351 tion by matching with the boundary layer solutions at either end of the fibre. Nu-  
 352 merical evaluation of the values of  $\bar{w}$  and  $\bar{R}$  in the far field yields

$$353 \quad (5.19) \quad \bar{w}(\bar{z} \rightarrow \infty) = c_w = -0.164,$$

$$354 \quad (5.20) \quad \bar{R}(\bar{z} \rightarrow \infty) = c_R = 0.082.$$

356 We note that far-field value of  $\bar{R}$  appears to be  $-1/2$  times the far-field value of  $\bar{w}$ .  
 357 In fact, this is an exact consequence of conservation of mass, which we can show as  
 358 follows. Integrating the no-flux condition (5.13) along the free surface yields

$$359 \quad (5.21) \quad \bar{R}(\bar{z} \rightarrow \infty) - \bar{R}(\bar{z} \rightarrow 0) = \int_0^\infty \bar{u}(1, \bar{z}) \, d\bar{z}.$$

360 Similarly, integrating the conservation of mass equation (5.6) over the entire boundary  
 361 layer yields

$$362 \quad (5.22) \quad \int_0^\infty \bar{u}(1, \bar{z}) \, d\bar{z} = -\frac{1}{2} [\bar{w}(\bar{z} \rightarrow \infty) - \bar{w}(\bar{z} = 0)]$$

363 since the  $\bar{w}$  is independent of  $\bar{z}$  at both ends. It then follows that  $c_R = -c_w/2$ .

364 **6. Corrections to the Trouton model.** From §4, the  $O(\epsilon)$  corrections  $w_1$  and  
 365  $R_1$  to the leading-order solution are given by (4.10), which can be rewritten using the  
 366 leading-order solutions (4.6)—(4.9) as

$$367 \quad (6.1) \quad \frac{d}{dz} \left( D^{-z} w_1 + 2D^{z/2} R_1 \right) = 0,$$

$$368 \quad (6.2) \quad \frac{d}{dz} \left[ 3 \left( D^{-z} \frac{dw_1}{dz} + 2 \ln(D) D^{z/2} R_1 \right) \right] = 0.$$

369

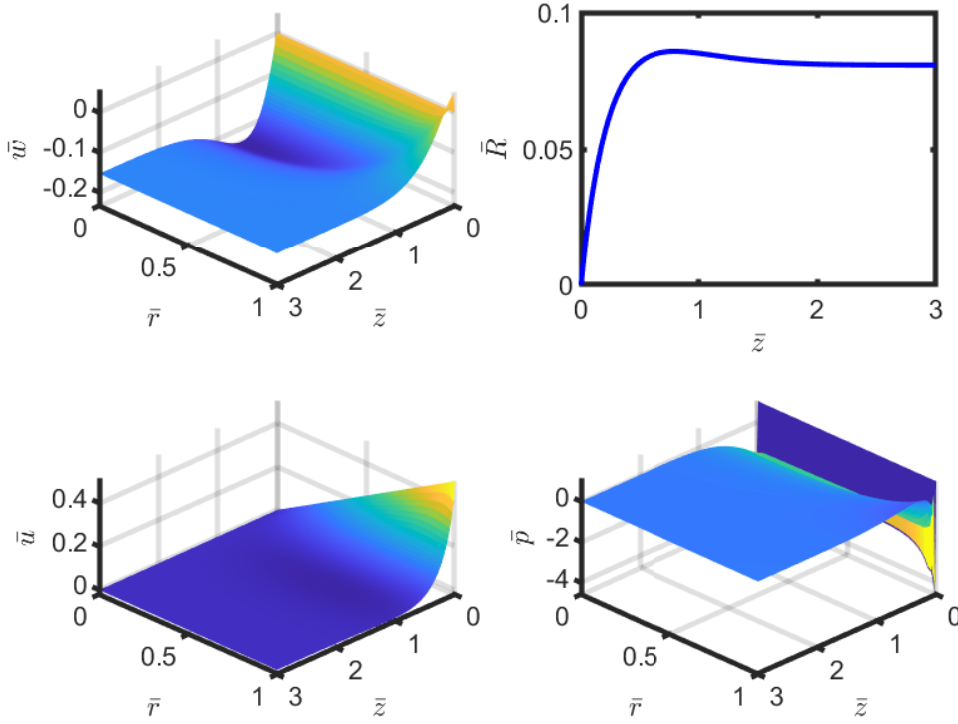


Fig. 6: Numerical solutions for  $\bar{w}$ ,  $\bar{u}$ ,  $\bar{R}$  and  $\bar{p}$  from the boundary-layer problem (5.6)—(5.13).

370 From §5.3, the corresponding boundary conditions are

$$371 \quad (6.3) \quad w_1 \rightarrow \ln(D)c_w, \quad R_1 \rightarrow -\frac{1}{2} \ln(D)c_w \quad \text{at } z \rightarrow 0,$$

$$372 \quad (6.4) \quad w_1 \rightarrow -D^{\frac{1}{2}} \ln(D)c_w \quad \text{at } z \rightarrow 1,$$

374 The problem is satisfied by

$$375 \quad (6.5) \quad w_1(z) = \ln(D)c_w \left[ 1 - \left( 1 + \frac{1}{\sqrt{D}} \right) z \right] D^z,$$

$$376 \quad (6.6) \quad R_1(z) = -\frac{1}{2} \ln(D)c_w \left[ 1 - \left( 1 + \frac{1}{\sqrt{D}} \right) z \right] D^{-z/2}.$$

378 We compare these correction terms with the difference between the numerical and  
 379 leading-order solutions for  $\epsilon = 0.1$  in Figure 4. We note that the numerical solution  
 380 uses the same boundary conditions (2.18)—(2.19) as the asymptotic analysis. The  
 381 correction  $\epsilon w_1$  is in excellent agreement with the estimate, except for in the boundary  
 382 layers where discrepancies should be expected. The literature prediction from [27] is  
 383 shown for comparison, and is both qualitatively and quantitatively different to the  
 384 observed behaviour. The scaled differences  $(w - w_0)/\epsilon$  collapse onto the single curve  
 385  $w_1$  for many values of  $\epsilon$  in Figure 7.

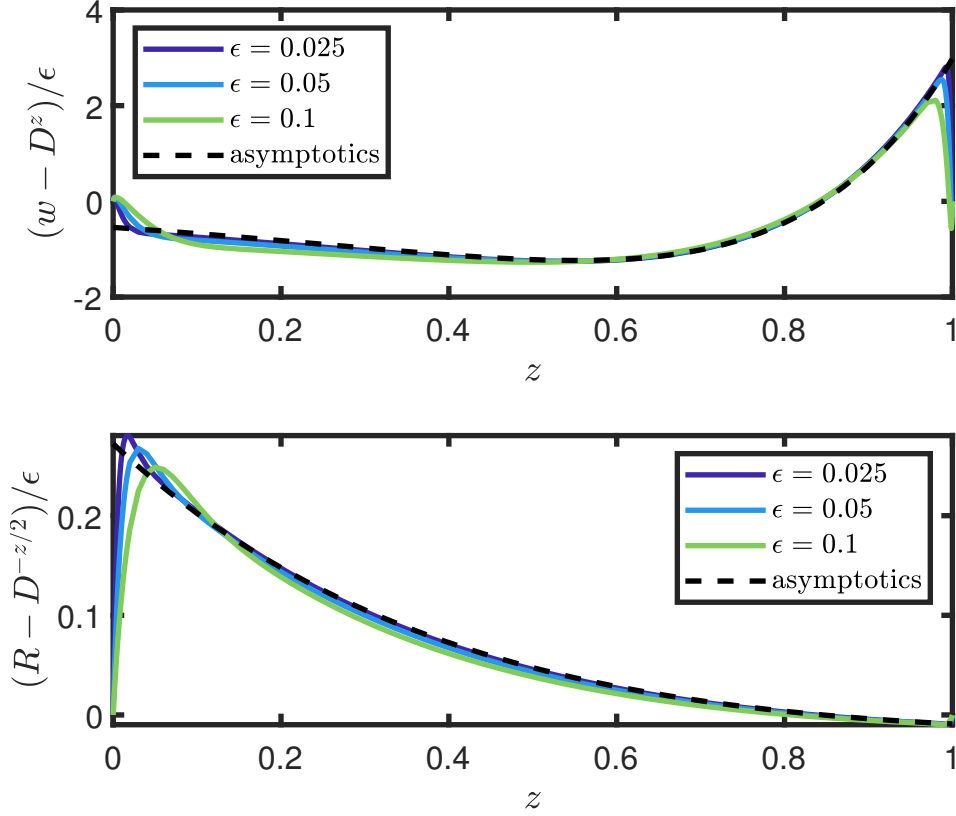


Fig. 7: Scaled difference between numerical and leading-order solutions, collapsed onto asymptotic solution (6.5)–(6.6).

386 The asymptotic approximation in the bulk of the sheet in the limit  $\epsilon \rightarrow 0$  can  
 387 now be written

(6.7)

$$388 \quad w(r, z) = D^z \left\{ 1 + \epsilon c_w \ln(D) \left[ 1 - \left( 1 + \frac{1}{\sqrt{D}} \right) z \right] \right\} + O(\epsilon^2),$$

(6.8)

$$389 \quad R(z) = D^{-z/2} \left\{ 1 - \epsilon \frac{c_w}{2} \ln(D) \left[ 1 - \left( 1 + \frac{1}{\sqrt{D}} \right) z \right] \right\} + O(\epsilon^2),$$

(6.9)

$$390 \quad u(r, z) = -\frac{r}{2} \ln(D) D^z \left\{ 1 + \epsilon c_w \left[ \ln(D) - \left( 1 + \frac{1}{\sqrt{D}} \right) (1 + \ln(D)z) \right] \right\} + O(\epsilon^2),$$

(6.10)

$$391 \quad p(r, z) = -\ln(D) D^z \left\{ 1 + \epsilon c_w \left[ \ln(D) - \left( 1 + \frac{1}{\sqrt{D}} \right) (1 + \ln(D)z) \right] \right\} + O(\epsilon^2). \\ 392$$

393 We note that the approximation (6.7)–(6.10) breaks down in boundary layers

394 near the inlet and outlet, and so should not be evaluated directly at  $z = 0$  and  $z = 1$ .  
 395 To evaluate the final fibre radius we revisit the outlet boundary layer expansion (5.16).  
 396 Matching with the bulk solution as  $z \rightarrow 1$ , we find that the offset constant  $c_{out} = 0$   
 397 and so the final fibre radius is  $1/\sqrt{D}$ , as expected. We can now construct composite  
 398 solutions  
 399

$$400 \quad (6.11a) \quad w(r, z) \approx D^z + \epsilon c_w \ln D \left\{ \left[ 1 - \left( 1 + \frac{1}{\sqrt{D}} \right) z \right] D^z + \right. \\ \left. \left[ \frac{\bar{w}(r, z/\epsilon)}{c_w} - 1 \right] - \sqrt{D} \left[ \frac{\bar{w}(r, \sqrt{D}(1-z)/\epsilon)}{c_w} - 1 \right] \right\},$$

401  
402  
403  
404

$$405 \quad (6.11b) \quad R(z) \approx D^{-z/2} - \epsilon \frac{c_w}{2} \ln D \left\{ \left[ 1 - \left( 1 + \frac{1}{\sqrt{D}} \right) z \right] D^{-z/2} \right. \\ \left. - \left[ 1 + \frac{\bar{R}(z/\epsilon)}{c_w/2} \right] + \frac{1}{D} \left[ 1 + \frac{\bar{R}(\sqrt{D}(1-z)/\epsilon)}{c_w/2} \right] \right\},$$

406  
407

408 which approximate the solution along the entire length of the fibre. This composite  
 409 solution is shown in Figure 8 for an aspect ratio  $\epsilon = 0.1$  and draw ratio  $D = 30$ .  
 410 The numerical, leading-order and composite solutions for the axial velocity are in-  
 411 distinguishable on the scale of the plot, but there is a clear discrepancy between the  
 412 numerical and leading-order solutions for the fibre radius, which is captured perfectly  
 413 by the composite solution.

## 414 7. Alternative boundary conditions.

415 **7.1. Stress condition.** When the leading-order velocity vector in the bulk of  
 416 the sheet cannot satisfy the boundary conditions, boundary layers must be introduced  
 417 at the sheet ends. In [27], the existence and importance of the boundary layers was  
 418 obscured by the application of cross-sectionally averaged boundary conditions, which  
 419 allowed for the derivation of a solution with no  $O(\epsilon)$  corrections, and instead  $O(\epsilon^2)$   
 420 terms were presented. Even though applying a uniform axial stress and zero shear  
 421 stress eliminates the  $O(\epsilon)$  corrections, the corresponding  $O(\epsilon^2)$  corrections do not  
 422 match those in [27]. This can be understood by noting that Eq. (4.12) is of the form  
 423  $w_2 = a(z)r^2 + b(z)$ ; this  $r$ -dependence still must be resolved across boundary layers if  
 424 the inlet velocity is uniform, which in turn alters the boundary conditions required  
 425 to determine  $a$  and  $b$ . The asymptotic analysis required to determine the corrections  
 426 is likely to have industrial relevance and may therefore warrant further exploration in  
 427 the future.

428 **7.2. Poiseuille flow.** In §2.2, we considered the possibility of Poiseuille flow  
 429 inlet conditions. Here, the leading order axial velocity has radial dependence, and is  
 430 incompatible with the leading-order Trouton flow profile. A different boundary-layer  
 431 analysis is required to account for this, and indeed for any inlet condition where the  
 432 axial velocity has radial dependence at leading order. In particular, the axial velocity  
 433 would need to change by an  $O(1)$  amount in the bulk, and this in turn would require  
 434 that the radial velocity is an order of magnitude larger, and the appropriate scalings  
 435 would be

$$436 \quad (7.1) \quad z = \epsilon \tilde{z}, \quad w = \epsilon^{-1} \tilde{w}, \quad p = \epsilon^{-1} \tilde{p}.$$

437 In this scenario the increased radial velocity may induce an  $O(1)$  change in the fibre  
 438 radius. By conservation of mass, this would mean that the uniform axial velocity  
 439 as the fibre exits the boundary layer would take a value other than 1. As such, the

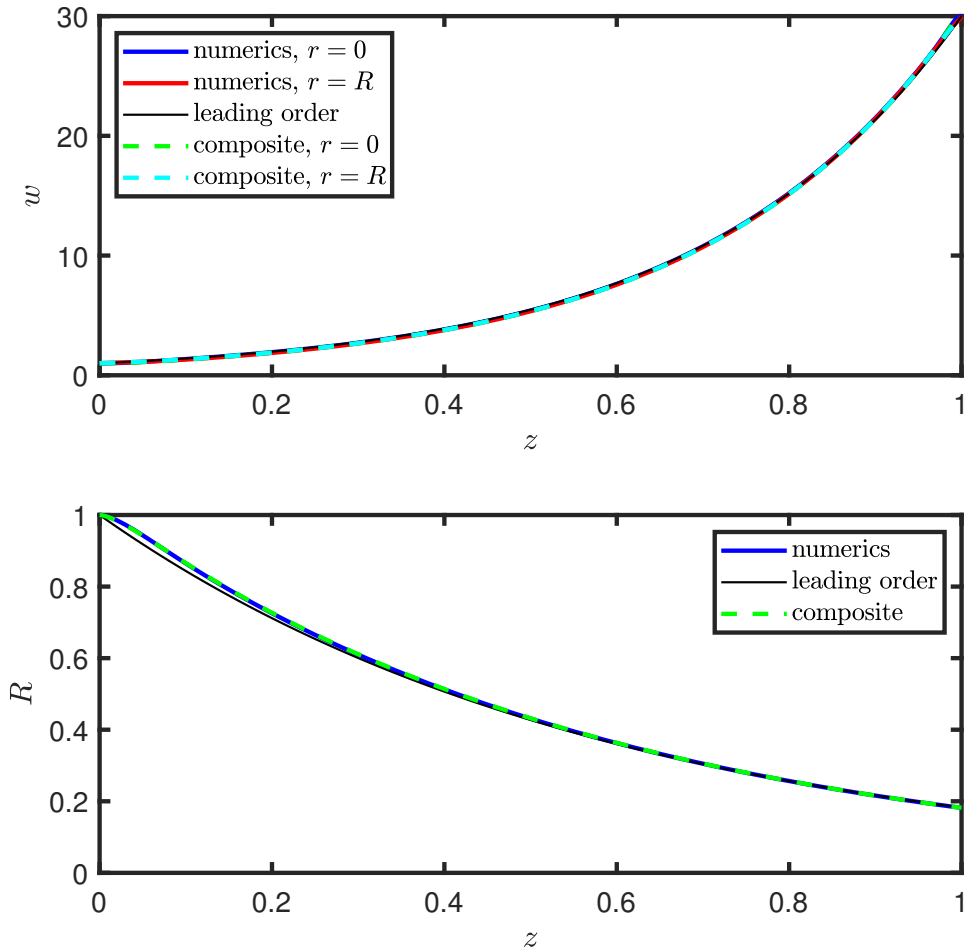


Fig. 8: Comparison between composite solution (6.11) and the numerical solution to (2.12)–(2.17) for aspect ratio  $\epsilon = 0.1$  and draw ratio  $D = 30$ .

440 leading-order solution may change quantitatively. However, it seems reasonable to  
 441 anticipate that the appropriate asymptotic expansion will proceed in powers of  $\epsilon$ , as  
 442 it does for the problem considered here. Again, this scenario may warrant further  
 443 investigation in the future.

444 **8. Temperature effects.** In drawing processes, the viscosity of the viscous fluid  
 445 may vary significantly due to changes in temperature (see e.g. [29, 28]). In the simplest  
 446 cases, heat transfer to the fluid is strong so that the temperature (and hence viscosity)  
 447 can be treated as functions of  $z$  only, which are not coupled to the flow profile. The  
 448 corresponding governing equations and approximate asymptotic solution for a small  
 449 aspect ratio are modified only slightly provided the change in viscosity is not too  
 450 extreme, as outlined in Appendix A.

451 Elsewhere in the literature, in [23] a fibre drawing model is presented with a two-  
 452 way coupling between temperature and velocity. The authors consider the parameter

453 regime  $\epsilon \text{Pe}/\text{Bi} = 1$ , where  $\text{Pe}$  is the Péclet number,  $\text{Bi}$  is the Biot number, and  
 454 the temperature varies across the fibre radius at leading order. Making an *ad hoc*  
 455 assumption of a parabolic temperature profile allows the leading-order velocity to be  
 456 described in terms of an averaged temperature, and a correction associated with the  
 457 leading-order radial dependence of the viscosity is then computed. Although the role  
 458 of radially-varying temperature appears to be resolved accurately, the mathematical  
 459 derivation has some shortcomings: the assumed temperature profile does not satisfy  
 460 the heat equation, and the velocity is expanded in powers of  $\epsilon$  but the fibre radius  
 461 and temperature are not, so the contributions associated with these are not included.

462 **9. Discussion.** In this paper we analyse a mathematical model for fibre drawing  
 463 based on the assumption that the aspect ratio  $\epsilon \rightarrow 0$ . Our central result is that  
 464 corrections to the leading-order Trouton model are different for different boundary  
 465 conditions, are different to those previously reported in the literature for the boundary  
 466 conditions considered here, and scale linearly with  $\epsilon$  in the case of applied velocity  
 467 conditions. We calculated these corrections using a combination of boundary-layer  
 468 analysis and numerical methods, and hence derived composite solutions accurate to  
 469  $O(\epsilon^2)$ , as well as the correct axial tension required to attain a particular draw ratio.

470 The asymptotic structure can be summarized as follows. The leading-order axial  
 471 velocity does not vary radially, and increases exponentially between its inlet and  
 472 outlet values. The radial velocity is an order of magnitude smaller, and at leading  
 473 order is linear in  $r$ : this is incompatible with boundary conditions that include zero  
 474 radial velocity, and so the velocity profile in the fibre must adjust to its bulk profile  
 475 over boundary layers near the inlet and outlet whose size scales with the fibre radius.  
 476 The dynamics in the boundary layers can be described by a single canonical system  
 477 of partial differential equations, independent of both aspect ratio  $\epsilon$  and draw ratio  $D$ .  
 478 The matching conditions for the bulk for any system can then be determined by an  
 479 appropriate rescaling. These matching conditions necessitate the introduction of  $O(\epsilon)$   
 480 corrections to the bulk flow. This result demonstrates that simply applying averaged  
 481 boundary conditions to averaged bulk quantities leads to the loss of important infor-  
 482 mation about the fibre dynamics. The  $O(\epsilon)$  corrections are in excellent agreement  
 483 with numerical solutions to the full axisymmetric fibre description. If stress boundary  
 484 conditions are applied instead of the velocity conditions considered in the main part  
 485 of the paper, then the corrections to the leading order description are  $O(\epsilon^2)$ , but a  
 486 boundary-layer analysis is still required to determine the correct boundary conditions  
 487 for the  $O(\epsilon^2)$  equations.

488 The requirement for boundary-layer analysis and  $O(\epsilon)$  correction terms is not  
 489 unique to the scenario studied here. An analogous asymptotic structure and calcu-  
 490 lation of corrections was presented in [21] for drawing of a viscous sheet. The  
 491 occurrence of this phenomenon across multiple geometries suggests the existence of  
 492 a ubiquitous phenomenon whereby any extensional flow profile has two-dimensional  
 493 boundary layers where the flow profile adjusts to its one-dimensional bulk profile. Be-  
 494 yond Newtonian fluids, long-and-slender sheets and fibres exist in a plethora of other  
 495 real-world scenarios. For cereal extrusion, the difference between numerics and the  
 496 leading-order long-and-thin solution for extrusion of a compressible fluid was found  
 497 to scale linearly with aspect ratio as opposed to quadratically in [19], although the  
 498 corresponding boundary layer has not yet been analysed. Viscoelastic fluids are also  
 499 common in drawing and spinning, and the boundary-layer structure outlined here may  
 500 be useful for giving insight into aspects of these processes such as die swell, whereby  
 501 the fibre radius increases directly below the inlet before subsequently decreasing [1, 3].

502 Finally, this approach could also prove useful for scenarios involving plastic flow, such  
503 as metal sheet rolling [2].

504 **Appendix A. Analysis for axially varying viscosity.**

505 **A.1. Dimensionless model.** Here we consider an axially varying viscosity. We  
506 scale the dimensional viscosity with a typical value  $\mu^*$ , and define a dimensionless  
507 viscosity  $\mu = \mu(z)$ . The dimensionless governing equations (2.12)–(2.19) in this case  
508 are as follows. In the bulk,

509 (A.1) 
$$\frac{1}{r} \frac{\partial}{\partial r} (ru) + \frac{\partial w}{\partial z} = 0,$$

510 (A.2) 
$$\frac{1}{r} \frac{\partial}{\partial r} \left[ r \left( -p + 2\mu \frac{\partial u}{\partial r} \right) \right] - \frac{1}{r} \left( -p + 2\mu \frac{u}{r} \right) + \frac{\partial}{\partial z} \left( \mu \frac{\partial w}{\partial r} + \epsilon^2 \mu \frac{\partial u}{\partial z} \right) = 0,$$

511 (A.3) 
$$\frac{1}{r} \frac{\partial}{\partial r} \left[ r \left( \epsilon^{-2} \mu \frac{\partial w}{\partial r} + \mu \frac{\partial u}{\partial z} \right) \right] + \frac{\partial}{\partial z} \left( -p + 2\mu \frac{\partial w}{\partial z} \right) = 0.$$

513 At the free boundary  $r = R(z)$ ,

514 (A.4) 
$$u = \frac{dR}{dz} w,$$

515 (A.5) 
$$-p + 2\mu \frac{\partial u}{\partial r} = \frac{dR}{dz} \left( \mu \frac{\partial w}{\partial r} + \epsilon^2 \mu \frac{\partial u}{\partial z} \right),$$

516 (A.6) 
$$\epsilon^{-2} \mu \frac{\partial w}{\partial r} + \mu \frac{\partial u}{\partial z} = \frac{dR}{dz} \left( -p + 2\mu \frac{\partial w}{\partial z} \right),$$

518 and at the inlet and outlet

519 (A.7) 
$$w = 1, \quad u = 0, \quad R = 1 \text{ at } z = 0,$$

520 (A.8) 
$$w = D, \quad u = 0 \quad \text{at } z = 1.$$

522 The cross-averaged mass and momentum equations are

523 (A.9) 
$$\frac{d}{dz} \int_0^{R(z)} r w \, dr = 0,$$

524 (A.10) 
$$\frac{d}{dz} \int_0^{R(z)} r \left[ -p + 2\mu \frac{\partial w}{\partial z} \right] \, dr = 0.$$

526 **A.2. Bulk equations.** Repeating the analysis of §4.1, the  $O(1)$  quantities obey

527 (A.11) 
$$w_0 = W_0(z), \quad u_0 = -\frac{r}{2} W_0'(z), \quad p_0 = -\mu W_0'(z),$$

528 (A.12) 
$$\frac{d}{dz} (R_0^2 W_0) = 0, \quad \frac{d}{dz} (3\mu R_0^2 W_0') = 0,$$

529 (A.13) 
$$W_0(0) = 1, \quad R_0(0) = 1, \quad W_1(1) = D,$$

531 and thus are given by

532 (A.14) 
$$w_0 = D^Z,$$

533 (A.15) 
$$R_0 = D^{-Z/2},$$

534 (A.16) 
$$u_0 = -\frac{r \ln(D)}{2} \frac{1}{M} D^Z,$$

535 (A.17) 
$$p_0 = -\frac{\ln(D)}{M} D^Z,$$

536

537 where

$$538 \quad (A.18) \quad Z(z) = \frac{1}{M} \int_0^z \frac{1}{\mu(z')} dz' \in [0, 1]$$

539 is a modified axial variable, with  $M = \int_0^1 \frac{1}{\mu(z')} dz'$ .

540 Meanwhile, the  $O(\epsilon)$  quantities obey

$$541 \quad (A.19) \quad w_1 = W_1(z), \quad u_1 = -\frac{r}{2} W_1'(z), \quad p_1 = -\mu W_1'(z),$$

$$542 \quad (A.20) \quad \frac{d}{dz} (R_0^2 W_1 + 2R_0 R_1 W_0) = 0, \quad \frac{d}{dz} [3\mu (R_0^2 W_1' + 2R_0 R_1 W_0')] = 0,$$

544 and, as in §5 and §6, the description of the  $O(\epsilon)$  corrections must be completed by  
545 considering boundary layers near the inlet and outlet.

546 **A.3. Boundary layer analysis.** We resolve the boundary layers near the inlet  
547 and outlet via the rescalings

$$548 \quad (A.21a) \quad z = \epsilon \bar{z}, \quad r = \bar{r},$$

549 and

$$550 \quad (A.21b) \quad z = 1 - \epsilon D^{-1/2} \bar{z}, \quad r = D^{-1/2} \bar{r}$$

551 respectively. We assume that the viscosity varies on the global axial lengthscale in  
552 the bulk of the domain, but account for the possibility that it may also vary inside of  
553 the boundary layers by defining

$$554 \quad (A.22) \quad \bar{\mu}(\bar{z}) = \mu(z).$$

555 The modified axial coordinate  $Z$  should also be rescaled near the inlet and outlet via

$$556 \quad (A.23a) \quad Z(0 + \epsilon \bar{z}) = \frac{\epsilon}{M} \int_0^{\bar{z}} \frac{1}{\bar{\mu}(\bar{z}')} dz' = \frac{\epsilon}{M} \bar{Z}$$

557 and

$$558 \quad (A.23b) \quad Z(1 - \epsilon D^{-1/2} \bar{z}) = \frac{1}{M} \int_0^1 \frac{1}{\mu} dz - \frac{\epsilon D^{-1/2}}{M} \int_0^{\bar{z}} \frac{1}{\bar{\mu}(\bar{z}')} dz' = 1 - \frac{\epsilon D^{-1/2}}{M} \bar{Z}$$

559 respectively. We note that  $d\bar{Z}/d\bar{z} = 1/\bar{\mu}(\bar{z})$  in both boundary layers.

560 We can now propose boundary-layer solutions, analogous to those given by equa-  
561 tions (5.2)—(5.5) and (5.15)—(5.18). For simplicity, we use conservation of mass to  
562 assume that  $\bar{R}(1) = 1/\sqrt{D}$ , and use solutions of the form

$$563 \quad (A.24) \quad w(r, z) = 1 + \epsilon \frac{\ln(D)}{M} (\bar{Z} + \bar{w}(\bar{r}, \bar{z})) + \dots,$$

$$564 \quad (A.25) \quad R(z) = 1 + \epsilon \frac{\ln(D)}{M} \left( -\frac{\bar{Z}}{2} + \bar{R}(\bar{z}) \right) + \dots,$$

$$565 \quad (A.26) \quad u(r, z) = \frac{\ln(D)}{M} \left( -\frac{\bar{r}}{2\bar{\mu}} + \bar{u}(\bar{r}, \bar{z}) \right) + \dots,$$

$$566 \quad (A.27) \quad p(r, z) = \frac{\ln(D)}{M} (-1 + \bar{p}(\bar{r}, \bar{z})) + \dots.$$

567

568 near the inlet, and of the form

$$569 \quad (A.28) \quad w(r, z) = D \left[ 1 - \epsilon D^{-1/2} \frac{\ln(D)}{M} (\bar{Z} + \bar{w}(\bar{r}, \bar{z})) + \dots \right],$$

$$570 \quad (A.29) \quad R(z) = D^{-1/2} \left[ 1 - \epsilon D^{-1/2} \frac{\ln(D)}{M} \left( -\frac{\bar{Z}}{2} + \bar{R}(\bar{z}) \right) + \dots \right],$$

$$571 \quad (A.30) \quad u(r, z) = D^{1/2} \frac{\ln(D)}{M} \left( -\frac{\bar{r}}{2\bar{\mu}} + \bar{u}(\bar{r}, \bar{z}) \right) + \dots,$$

$$572 \quad (A.31) \quad p(r, z) = D \frac{\ln(D)}{M} (-1 + \bar{p}(\bar{r}, \bar{z})) + \dots,$$

574 near the outlet. Substituting these into the governing equations (A.21) yields a system  
575 of boundary-layer equations

$$576 \quad (A.32) \quad \frac{1}{\bar{r}} \frac{\partial}{\partial \bar{r}} (\bar{r} \bar{u}) + \frac{\partial \bar{w}}{\partial \bar{z}} = 0,$$

$$577 \quad (A.33) \quad \frac{1}{\bar{r}} \frac{\partial}{\partial \bar{r}} \left[ \bar{r} \left( -\bar{p} + 2\bar{\mu} \frac{\partial \bar{u}}{\partial \bar{r}} \right) \right] - \frac{1}{\bar{r}} \left( -\bar{p} + 2\bar{\mu} \frac{\bar{u}}{\bar{r}} \right) + \frac{\partial}{\partial \bar{z}} \left( \bar{\mu} \frac{\partial \bar{w}}{\partial \bar{r}} + \bar{\mu} \frac{\partial \bar{u}}{\partial \bar{z}} \right) = 0,$$

$$578 \quad (A.34) \quad \frac{1}{\bar{r}} \frac{\partial}{\partial \bar{r}} \left[ \bar{r} \left( \bar{\mu} \frac{\partial \bar{w}}{\partial \bar{r}} + \bar{\mu} \frac{\partial \bar{u}}{\partial \bar{z}} \right) \right] + \frac{\partial}{\partial \bar{z}} \left( -\bar{p} + 2\bar{\mu} \frac{\partial \bar{w}}{\partial \bar{z}} \right) = 0,$$

580 which are modification of the canonical free-boundary problem (5.6)–(5.8) for uni-  
581 form viscosity. The free-boundary conditions (A.22) are now

$$582 \quad (A.35) \quad \bar{u} = \frac{d\bar{R}}{d\bar{z}} \bar{w},$$

$$583 \quad (A.36) \quad -\bar{p} + 2\bar{\mu} \frac{\partial \bar{u}}{\partial \bar{r}} = 0,$$

$$584 \quad (A.37) \quad \bar{\mu} \frac{\partial \bar{w}}{\partial \bar{r}} + \bar{\mu} \frac{\partial \bar{u}}{\partial \bar{z}} = 0,$$

586 at  $\bar{r} = 1$ , which is again a slight modification of the uniform-viscosity case, and the  
587 boundary conditions at  $\bar{z} = 0$  are

$$588 \quad (A.38) \quad \bar{w} = \bar{R} = 0, \quad \bar{u} = \frac{\bar{r}}{2\bar{\mu}}.$$

589 We anticipate that the far-field values of  $\bar{w}$  and  $\bar{R}$  may be different for different  
590 viscosity profiles  $\bar{\mu}(\bar{z})$  and therefore may be different for the inlet and outlet problems,  
591 so we introduce corresponding notation

$$592 \quad (A.39a) \quad \bar{w}(\bar{r}, \bar{z} \rightarrow \infty; \mu^{(in)}) = -2\bar{R}(\bar{z} \rightarrow \infty; \mu^{(in)}) = c_w^{(in)},$$

593

$$594 \quad (A.39b) \quad \bar{w}(\bar{r}, \bar{z} \rightarrow \infty; \mu^{(out)}) = -2\bar{r}(\bar{z} \rightarrow \infty; \mu^{(out)}) = c_w^{(out)}.$$

595 **A.4. Resolving bulk and boundary layers.** Solving the governing equa-  
596 tions (A.20) subject to boundary conditions

$$597 \quad (A.40a) \quad w_1 = c_w^{(in)} \frac{\ln(D)}{M}, \quad R_1(\bar{z} \rightarrow \infty) = -\frac{c_w^{(in)}}{2} \frac{\ln(D)}{M} \quad \text{at } z = 0,$$

598

$$599 \quad (\text{A.40b}) \quad w_1 = -c_w^{(out)} \sqrt{D} \frac{\ln(D)}{M} \quad \text{at } z = 1$$

600 yields finally a modified set of corrections

$$601 \quad (\text{A.41}) \quad w_1 = D^Z \frac{\ln(D)}{M} \left[ c_w^{(in)} - \left( c_w^{(in)} + \frac{c_w^{(out)}}{\sqrt{D}} \right) Z \right],$$

$$602 \quad (\text{A.42}) \quad R_1 = -\frac{1}{2} D^{-Z/2} \frac{\ln(D)}{M} \left[ c_w^{(in)} - \left( c_w^{(in)} + \frac{c_w^{(out)}}{\sqrt{D}} \right) Z \right],$$

$$603 \quad (\text{A.43}) \quad u_1 = -\frac{r}{2\mu} \frac{\ln(D)}{M^2} D^Z \left[ \ln(D) c_w^{(in)} - \left( c_w^{(in)} + \frac{c_w^{(out)}}{\sqrt{D}} \right) (1 + \ln(D)Z) \right],$$

$$604 \quad (\text{A.44}) \quad p_1 = -\frac{\ln(D)}{M^2} D^Z \left[ \ln(D) c_w^{(in)} - \left( c_w^{(in)} + \frac{c_w^{(out)}}{\sqrt{D}} \right) (1 + \ln(D)Z) \right].$$

605

606 We can thus see that an axially varying viscosity changes the solution quantitatively,  
 607 but does not change the qualitative behaviour and in particular does not affect the  
 608 boundary layer structure. However, we note that the length of the boundary layer  
 609 will decrease as  $\mu$  increases, so if  $\mu$  changes by many orders of magnitude and cannot  
 610 be treated as  $O(1)$ , then this analysis would break down and an alternative approach  
 611 would be needed. This is relevant in some glass drawing scenarios [20] and so may  
 612 warrant further investigation in the future.

### 613 **Appendix B. Numerical solutions.**

614 It is easier to write the governing equations in weak form if the momentum balance  
 615 is written in the form  $\nabla \cdot \boldsymbol{\sigma} = \mathbf{0}$  where  $\boldsymbol{\sigma}$  is the stress tensor, i.e.

$$616 \quad (\text{B.1a}) \quad \frac{1}{r} \frac{\partial}{\partial r} \left[ r \left( -p + 2 \frac{\partial u}{\partial r} \right) \right] - \frac{1}{r} \left( -p + 2 \frac{u}{r} \right) + \frac{\partial}{\partial z} \left( \epsilon^2 \frac{\partial u}{\partial z} + \frac{\partial w}{\partial r} \right) = 0,$$

617

$$618 \quad (\text{B.1b}) \quad \frac{1}{r} \frac{\partial}{\partial r} \left[ r \left( \frac{\partial u}{\partial z} + \epsilon^{-2} \frac{\partial w}{\partial r} \right) \right] + \frac{\partial}{\partial z} \left( -p + 2 \frac{\partial w}{\partial z} \right) = 0.$$

619 We map the problem onto a fixed domain by making a change of variables

$$620 \quad (\text{B.2}) \quad \eta = \frac{r}{R(z)}, \quad \zeta = z,$$

621 to map the problem onto a fixed domain  $(\eta, \zeta) \in [0, 1] \times [0, 1]$ . We thus rewrite  
 622 derivatives using the chain rule as

$$623 \quad (\text{B.3}) \quad \frac{\partial}{\partial r} = \frac{1}{R(\zeta)} \frac{\partial}{\partial \eta}, \quad \frac{\partial}{\partial z} = \frac{\partial}{\partial \zeta} - \frac{R'(\zeta)}{R(\zeta)} \eta \frac{\partial}{\partial \eta}.$$

624 Substituting this change of variables into the mass and momentum equations (2.12)  
 625 and (B.1a)—(B.1b) yields

$$626 \quad (\text{B.4a}) \quad \frac{1}{R} \frac{1}{\eta} \frac{\partial}{\partial \eta} (\eta u) + \frac{\partial w}{\partial \zeta} - \frac{R'}{R} \eta \frac{\partial w}{\partial \eta} = 0,$$

627  
628

$$(B.4b) \quad \frac{1}{R} \frac{1}{\eta} \frac{\partial}{\partial \eta} \left[ \eta \left( -p + 2 \frac{1}{R} \frac{\partial u}{\partial \eta} \right) \right] - \frac{1}{R} \frac{1}{\eta} \left( -p + 2 \frac{1}{R} \frac{\partial u}{\partial \eta} \right) \\ + \left( \frac{\partial}{\partial \zeta} - \frac{R'(\zeta)}{R(\zeta)} \eta \frac{\partial}{\partial \eta} \right) \left[ \epsilon^2 \left( \frac{\partial u}{\partial \zeta} - \frac{R'(\zeta)}{R(\zeta)} \frac{\partial u}{\partial \eta} \right) + \frac{1}{R} \frac{\partial w}{\partial \eta} \right],$$

630  
631  
632  
633

$$(B.4c) \quad \frac{1}{R} \frac{1}{\eta} \frac{\partial}{\partial \eta} \left[ \eta \left( \frac{\partial u}{\partial \zeta} - \frac{R'(\zeta)}{R(\zeta)} \eta \frac{\partial u}{\partial \eta} + \epsilon^{-2} \frac{1}{R} \frac{\partial w}{\partial \eta} \right) \right] \\ + \left( \frac{\partial}{\partial \zeta} - \frac{R'(\zeta)}{R(\zeta)} \eta \frac{\partial}{\partial \eta} \right) \left[ -p + 2 \left( \frac{\partial w}{\partial \zeta} - \frac{R'(\zeta)}{R(\zeta)} \eta \frac{\partial w}{\partial \eta} \right) \right].$$

635  
636

637 The corresponding free-boundary conditions (2.15)–(2.17) become

$$(B.5) \quad u = R'(\zeta)w,$$

$$(B.6) \quad -p + 2 \frac{1}{R} \frac{\partial u}{\partial \eta} = R'(\zeta) \left[ \frac{1}{R} \frac{\partial w}{\partial \eta} + \epsilon^2 \left( \frac{\partial u}{\partial \zeta} - \frac{R'}{R} \eta \frac{\partial u}{\partial \eta} \right) \right],$$

$$(B.7) \quad \epsilon^{-2} \frac{1}{R} \frac{\partial w}{\partial \eta} + \left( \frac{\partial u}{\partial \zeta} - \frac{R'}{R} \eta \frac{\partial u}{\partial \eta} \right) = R'(z) \left[ -p + 2 \left( \frac{\partial w}{\partial \zeta} - \frac{R'}{R} \eta \frac{\partial w}{\partial \eta} \right) \right],$$

640  
641642 applied now at the fixed boundary  $\eta = 1$ . The inlet and outlet conditions remain  
643 unchanged and are

$$(B.8) \quad w = 1, \quad u = 0, \quad R = 1 \text{ at } \zeta = 0,$$

$$(B.9) \quad w = D, \quad u = 0 \quad \text{at } \zeta = 1.$$

644 We note that  $R(\zeta)$  is a function of one variable only and should, in principle, be  
645 solved in a different domain to the other variables. This complication is most simply  
646 avoided by treating  $R$  as a function of both  $\zeta$  and  $\eta$ , introducing a governing partial  
647 differential equation

$$(B.10) \quad \frac{\partial R}{\partial \eta} = 0$$

652 in the bulk of the domain, and replacing all instances of  $R'$  with  $\partial R / \partial \zeta$ .

653

## REFERENCES

- [1] J. BATCHELOR, J. BERRY, AND F. HORSFALL, *Die swell in elastic and viscous fluids*, *Polymer*, 14 (1973), pp. 297–299.
- [2] C. CAWTHORN, J. MINTON, AND E. BRAMBLEY, *Asymptotic analysis of cold sandwich rolling*, *Int. J. Mech. Sci.*, 106 (2016), pp. 184–193.
- [3] J. C. CHANG AND M. M. DENN, *An experimental study of isothermal spinning of a newtonian and viscoelastic liquid*, *J. Non-Newton. Fluid Mech.*, 5 (1979), pp. 369–385.
- [4] L. CUMMINGS AND P. HOWELL, *On the evolution of non-axisymmetric viscous fibres with surface tension, inertia and gravity*, *J. Fluid Mech.*, 389 (1999), pp. 361–389.
- [5] Y. DEMAY AND J.-F. AGASSANT, *An overview of molten polymer drawing instabilities*, *Int. Polym. Process.*, 29 (2014), pp. 128–139.
- [6] J. DEWYNNE, J. OCKENDON, AND P. WILMOTT, *A systematic derivation of the leading-order equations for extensional flows in slender geometries*, *J. Fluid Mech.*, 244 (1992), pp. 323–338.
- [7] R. J. FISHER, M. M. DENN, AND R. I. TANNER, *Initial profile development in melt spinning*, *Ind. Eng. Chem. Fundam.*, 19 (1980), pp. 195–197.

- 669 [8] A. D. FITT, K. FURUSAWA, T. M. MONRO, C. P. PLEASE, AND D. J. RICHARDSON, *The math-*  
670 *ematical modelling of capillary drawing for holey fibre manufacture*, J. Eng. Math., 43  
671 (2002), pp. 201–227.
- 672 [9] G. GEORGIU, L. OLSON, W. SCHULTZ, AND S. SAGAN, *A singular finite element for stokes*  
673 *flow: the stick-slip problem*, Int. J. Numer. Methods Fluids, 9 (1989), pp. 1353–1367.
- 674 [10] W. A. GIFFORD, *A finite element analysis of isothermal fiber formation*, Phys. Fluids, 25  
675 (1982), pp. 219–225.
- 676 [11] I. M. GRIFFITHS AND P. D. HOWELL, *The surface-tension-driven evolution of a two-dimensional*  
677 *annular viscous tube*, J. Fluid Mech., 593 (2007), pp. 181–208.
- 678 [12] I. M. GRIFFITHS AND P. D. HOWELL, *Mathematical modelling of non-axisymmetric capillary*  
679 *tube drawing*, J. Fluid Mech., 605 (2008), pp. 181–206.
- 680 [13] I. M. GRIFFITHS AND P. D. HOWELL, *The surface-tension-driven retraction of a viscida*, SIAM  
681 J. Appl. Math., 70 (2010), pp. 1453–1487.
- 682 [14] P. HOWELL, *Extensional thin layer flows*, PhD thesis, University of Oxford, 1994.
- 683 [15] J.-C. HYUN, *Draw resonance in polymer processing: a short chronology and a new approach*,  
684 Korea-Aust. Rheol. J., 11 (1999), pp. 279–285.
- 685 [16] H. G. LANDAU, *Heat conduction in a melting solid*, Q. Appl. Math., 8 (1950), pp. 81–94.
- 686 [17] A. LOGG, K.-A. MARDAL, AND G. WELLS, *Automated solution of differential equations by the*  
687 *finite element method: The FEniCS book*, vol. 84, Springer Science & Business Media,  
688 2012.
- 689 [18] M. A. MATOVICH AND J. R. A. PEARSON, *Spinning a molten threadline. steady-state isothermal*  
690 *viscous flows*, Ind. Eng. Chem. Fundam., 8 (1969), pp. 512–520.
- 691 [19] M. MCPHAIL, *Mathematical modelling of cereal extrusion*, PhD thesis, University of Oxford,  
692 2019.
- 693 [20] D. O’KIELY, C. J. W. BREWARD, I. M. GRIFFITHS, P. D. HOWELL, AND U. LANGE, *Edge*  
694 *behaviour in the glass sheet redraw process*, J. Fluid Mech., 785 (2015), pp. 248–269.
- 695 [21] D. O’KIELY, C. J. W. BREWARD, I. M. GRIFFITHS, P. D. HOWELL, AND U. LANGE, *Glass sheet*  
696 *redraw through a long heater zone*, IMA J. App. Math., 83 (2018), pp. 799–820.
- 697 [22] D. O’KIELY, C. J. W. BREWARD, I. M. GRIFFITHS, P. D. HOWELL, AND U. LANGE, *Out-of-plane*  
698 *buckling in two-dimensional glass drawing*, J. Fluid Mech., 869 (2019), pp. 587–609.
- 699 [23] A. G. PAGE, M. BECHERT, F. GALLAIRE, AND F. SORIN, *Unraveling radial dependency effects*  
700 *in fiber thermal drawing*, Appl. Phys. Lett., 115 (2019), p. 044102.
- 701 [24] J. R. A. PEARSON AND M. A. MATOVICH, *Spinning a molten threadline. stability*, Ing. Eng.  
702 Chem. Fundam., 8 (1969), pp. 605–609.
- 703 [25] C. J. S. PETRIE AND M. M. DENN, *Instabilities in polymer processing*, AIChE Journal, 22  
704 (1976), pp. 209–236.
- 705 [26] B. SCHEID, S. QUILIGOTTI, B. TRAN, R. GY, AND H. STONE, *On the (de) stabilization of draw*  
706 *resonance due to cooling*, J. Fluid Mech., 636 (2009), pp. 155–176.
- 707 [27] W. W. SCHULTZ AND S. H. DAVIS, *One-dimensional liquid fibers*, J. Rheol., 26 (1982), pp. 331–  
708 345.
- 709 [28] Y. STOKES, J. WYLIE, AND M. CHEN, *Coupled fluid and energy flow in fabrication of mi-*  
710 *crostructured optical fibres*, J. Fluid Mech., 874 (2019), pp. 548–572.
- 711 [29] M. TARONI, C. J. W. BREWARD, L. J. CUMMINGS, AND I. M. GRIFFITHS, *Asymptotic solutions*  
712 *of glass temperature profiles during steady optical fibre drawing*, J. Eng. Math., 80 (2013),  
713 pp. 1–20.
- 714 [30] A. TOKAREV, O. TROTSSENKO, I. GRIFFITHS, H. STONE, AND S. MINKO, *Magnet spinning of*  
715 *nano- and microfibers*, Advanced Materials, 27 (2015), pp. 3560–3565.
- 716 [31] F. TROUTON, *On the coefficient of viscous traction and its relation to that of viscosity*, Proc.  
717 Roy. Soc. A - Math. Phys., 77 (1906), pp. 426–440.